Siglecs-7/9 function as inhibitory immune checkpoints in vivo and can be targeted to enhance therapeutic antitumor immunity

Itziar Ibarlucea-Benitez[a], Polina Weitzenfeld[a], Patrick Smith[a], and Jeffrey V. Ravetch[a,1]

[a]Laboratory of Molecular Genetics and Immunology, The Rockefeller University, New York, NY 10065

Contributed by Jeffrey V. Ravetch, May 21, 2021 (sent for review April 19, 2021; reviewed by Diane Mathis and Tadatsugu Taniguchi)

Given the role of myeloid cells in T cell activation and in the antitumor response, targeting checkpoint molecules expressed on this population represents a promising strategy to augment antitumor immunity. However, myeloid checkpoints that can be effectively used as immunotherapy targets are still lacking. Here, we demonstrate the therapeutic potential of targeting the myeloid receptors Siglec-7 and Siglec-9 in vivo. By using a humanized immunocompetent murine model, we demonstrate that human Siglec-7 and Siglec-9, in addition to the murine homolog Siglec-E, inhibit the endogenous antitumor immune response, as well as the response to tumor-targeting and immune checkpoint inhibiting antibodies in vivo. The impact of these Siglecs on tumor progression is highly dependent on the anatomical distribution of the tumor and, as a consequence, the local tumor microenvironment, as tumors with a more immune-suppressive tumor microenvironment are less sensitive to Siglec perturbation. Finally, to assess the potential of these two receptors as targets for immunotherapy, we developed Fc engineered blocking antibodies to Siglec-7 and Siglec-9 and demonstrate that Siglec-7 and Siglec-9 blockade can significantly reduce tumor burden in vivo, demonstrating the therapeutic potential of targeting these two receptors.

cancer immunotherapy | checkpoint | Fc receptor | sialoglycan | Siglecs

Immune checkpoint modulators have been a major breakthrough in cancer therapy, starting with the approval of ipilimumab in 2011. Currently, there are seven Food and Drug Administration-approved immune checkpoint inhibitors (ICIs), all of them targeting the PD-1/PD-L1 axis or CTLA-4 on T cells (1–4). Despite the clinical success of these therapies, only about 25% of patients across all tumor indications respond to ICIs, suggesting that there are additional mechanisms that are important in driving antitumor immunity (5, 6). This limited efficacy underscores the importance of better understanding the mechanisms underlying the antitumor immune response, and the mechanisms that mediate response to ICIs, as well as identifying additional pathways to modulate it.

Given the pivotal role of myeloid cells in antitumor response in general and in T cell activation in particular, checkpoint molecules expressed on myeloid cells have emerged as potential therapeutic targets to promote antitumor immunity (7–11). Because of their immune-inhibitory nature, the family of Siglec (sialic acid-binding immunoglobulin-type lectins) receptors has been of particular interest for their potential as immune-modulatory targets (12–16). Siglecs are inhibitory receptors expressed almost exclusively on immune cells. They interact with sialoglycans, sialylated glycans that are expressed by most mammalian cells and are considered a marker of "self." The Siglec-sialoglycan axis is therefore an inhibitory pathway that protects the body from autoimmunity (17, 18). Up-regulation of sialoglycan expression, however, is commonly found on various tumor types (12, 13, 19, 20), and numerous studies have indicated that their interaction with Siglecs can inhibit immune cell activity, thus contributing to an immunosuppressive tumor microenvironment (TME) (21, 22). Thus, targeting Siglecs represents a promising therapeutic strategy to augment antitumor immunity.

In humans, the family of Siglec receptors comprises 15 members that vary in their expression pattern among the different immune cell types and in their specificity for sialic acid containing ligands. Based on sequence similarity, they can be divided into conserved Siglecs (Siglec-1, -2, -4, and -15), and rapidly evolving CD33-related Siglecs (CD33 or Siglec-3, Siglec-5, -6, -7, -8, -9, -10, -11, -12, -14, and -16) (17). In contrast to conserved Siglecs, CD33-related Siglecs do not have clear mammalian orthologs and exhibit a broader expression across the myeloid and lymphoid compartments (23). The CD33-related Siglec-7 and Siglec-9 are of particular interest in the context of tumor immunotherapy, as a variety of human cancers express ligands for both of these Siglecs, and recent evidence suggests that engagement of these two receptors attenuates both myeloid and lymphoid antitumor responses (12, 24–28). Siglec-7 and Siglec-9 are closely related: they share ∼98% amino acid sequence similarity, show a similar expression pattern across immune cells, and have similar ligand affinity (29). However, most of our mechanistic understanding of how these two Siglecs contribute to tumor progression comes from in vitro studies that lack the complexity of cellular and morphological diversity, and the interplay of soluble and cellular immune mediators found in vivo (24, 27, 30, 31). Additionally, the limited number of in vivo studies rely on the use of mouse models with mixed genetic backgrounds and have resulted in confounding and inconsistent conclusions (12, 13). Thus, the data reported to date fails to provide a comprehensive model of how

Significance

Targeting myeloid cells represents a promising strategy to augment antitumor immunity and overcome resistance to existing T cell-targeting therapies. However myeloid checkpoints that can be effectively used as immunotherapy targets are still lacking. Here, we demonstrate the therapeutic potential of targeting Siglec-7 and Siglec-9 to enhance antitumor immunity in vivo. Using an immunocompetent mouse model humanized for Siglec-7/9, we show that these receptors inhibit the endogenous antitumor immune response in a tissue-specific manner. These Siglecs also restrict the response to tumor-targeting and checkpoint-targeting antibodies, highlighting their significance in combinatorial approaches to immunotherapy. Finally, we show that Siglec-7/9 blockade can significantly reduce tumor burden in vivo, supporting the use of antibodies targeting Siglec-7/9 to therapeutically enhance antitumor immunity.

Author contributions: I.I.-B. and J.V.R. designed research; I.I.-B. performed research; P.W. and P.S. contributed new reagents/analytic tools; I.I.-B. and J.V.R. analyzed data; and I.I.-B. and J.V.R. wrote the paper.

Reviewers: D.M., Harvard Medical School; and T.T., University of Tokyo.

The authors declare no competing interest.

[1]To whom correspondence may be addressed. Email: ravetch@rockefeller.edu.

This article contains supporting information online at https://www.pnas.org/lookup/suppl/doi:10.1073/pnas.2107424118/-/DCSupplemental.

Published June 21, 2021.

Siglec-7 and Siglec-9 contribute to tumor progression, and in vivo evidence of their benefit in promoting antitumor immunity when targeted with therapeutic antibodies.

In this study, we investigated the impact of Siglec-7 and Siglec-9 on tumor progression using a humanized immunocompetent murine model, and investigated their potential role as therapeutic targets to promote antitumor immunity. Our data demonstrate that Siglec-7 and Siglec-9 inhibit the endogenous antitumor immune response, as well as the response to tumor-targeting and checkpoint-targeting antibodies in vivo. Using Fc-engineered anti–Siglec-7 and anti–Siglec-9 blocking antibodies, we show reduced tumor burden, thus demonstrating the therapeutic potential of targeting these two Siglecs to augment the antitumor immune response.

Results

Siglec-E Is Expressed in the TME. Siglec-E is the murine functional homolog of Siglec-9, while Siglec-7 does not have a known murine homolog (20). To determine if Siglec-E is able to inhibit the antitumor immune response by engaging ligands on tumor cells, we assessed the presence of Siglec-E ligands on murine tumor cell lines and the expression of Siglec-E on tumor-infiltrating leukocytes (TILs) of murine syngeneic tumors. To address the former, we analyzed the binding of a soluble Fc-fusion of Siglec-E (Siglec-E–Fc) to well-established and widely used murine tumor cell lines: B16F10 melanoma (B16), MC38 colon carcinoma, EL4 lymphoma, and ID8 ovarian carcinoma. All tested cell lines were found to express Siglec-E ligands and were able to bind Siglec-E (Fig. 1*A*). Next, we evaluated whether Siglec-E is expressed on TILs. We found that Siglec-E is primarily expressed on infiltrating neutrophils, macrophages, and dendritic cells (DCs) in both B16 and MC38 tumor model systems. Lower expression was observed on $CD4^+$ T cells and $CD8^+$ T cells, with $FoxP3^+$ $CD4^+$ T cells expressing higher levels of Siglec-E than $FoxP3^-CD4^+$ T cells, suggesting that Siglec-E expression on regulatory T cells (T_{regs}) could be important for its role in suppressing the adaptive immune response to tumors (Fig. 1*B*). Collectively, these data demonstrate prominent expression of the inhibitory Siglec-E on both innate and adaptive immune cells within the TME, as well as the presence of Siglec-E ligands on the surface of murine tumor cells, together facilitating the interaction between tumor and immune cells to promote tumor growth.

Generation of Mouse Models: Siglec-E Knockout and Humanized Siglec7$^+$/9$^+$/Siglec-E Knockout Mice. To study the contribution of Siglec-E to the immune response against the tumor, we generated an isogenic mouse model lacking this receptor (Siglec-E knockout [KO] mice). The Siglec-E KO mouse line was generated by deleting an 11-bp segment at the 3′ end of exon 3 of the Siglec-E gene in C57BL/6 mice, leading to a premature termination codon (Fig. 1*C*). We verified the lack of Siglec-E expression in this new mouse by flow cytometry: while naïve WT C57BL/6 mice express Siglec-E on neutrophils, inflammatory monocytes, macrophages, and DCs, Siglec-E KO mice lacked expression of the receptor in all tested immune populations (Fig. 1*D*). These mice develop normally, are fertile, and do not show evidence of any spontaneous pathology from loss of Siglec-E.

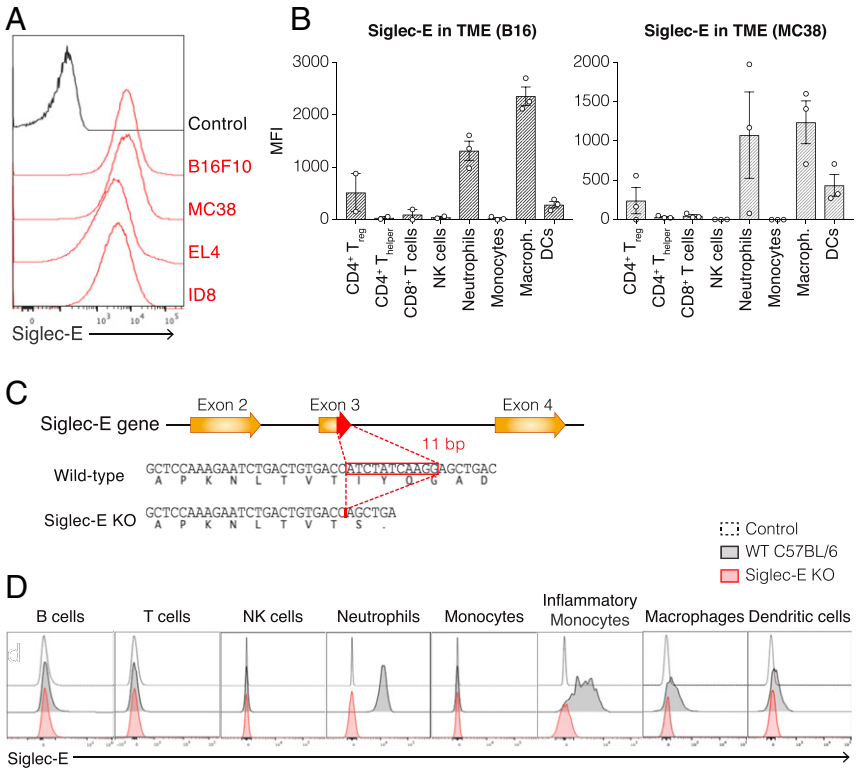

Fig. 1. Characterization of Siglec-E expression in the tumor microenvironment and validation of a Siglec-E KO mouse model. (*A*) Surface expression of Siglec-E ligands on murine tumor cell lines. Cells were incubated with a Siglec-E Fc chimera (mouse IgG), followed by PE-conjugated anti-mouse IgG secondary antibody. Panel shows a representative experiment ($n = 3$). (*B*) Expression of Siglec-E on immune populations infiltrated into B16 subcutaneous tumors (*Left*) or MC38 subcutaneous tumors (*Right*) in WT C57BL/6 mice. Graph shows median fluorescence intensity (MFI) of Siglec-E, each circle represents one mouse. Data are displayed as mean ± SEM. Panel shows a representative experiment ($n = 2$). (*C*) Siglec-E KO mouse line generation. Briefly, an 11-bp segment at the 3′ end of exon 3 of the Siglec-E gene was deleted, thereby introducing a premature termination codon. (*D*) Validation of Siglec-E KO mice: surface expression of Siglec-E on immune populations of WT C57BL/6 mice (black) or Siglec-E KO mice (red) compared to an unstained control (dashed line). Panel shows a representative mouse ($n > 9$).

In order to evaluate the role of the human Siglec-7 and Siglec-9 in tumor progression and their potential as therapeutic targets to improve antitumor immunity, we next generated an isogenic mouse model humanized for these two Siglecs on the Siglec-E KO background. First, we generated a mouse line carrying the human Siglec-7 and Siglec-9 under their human regulatory elements on a C57BL/6 background by introducing a 90-Kbp BAC transgene encoding both genes into C57BL/6 embryos (Siglec-7/9 mice) (Fig. 2*A*). Next, we crossed the resulting Siglec-7/9 transgenic mouse to the Siglec-E KO mouse strain described above to generate a humanized mouse model for Siglec-7/9 that lacks the mouse homolog Siglec-E (Siglec-7/9/Siglec-E KO mice). We evaluated the expression pattern of Siglec-7 and Siglec-9 on different immune populations in the humanized mice and compared it with the expression of these Siglecs in humans. Similar to the pattern found on human immune cells (*SI Appendix*, Fig. S1), both Siglec-7 and Siglec-9 are expressed on neutrophils, monocytes, macrophages, DCs, NK cells, and to a lesser extent on T cells in the Siglec-7/9/Siglec-E KO mice (Fig. 2 *B* and *C*). We further validated the Siglec-7/9/Siglec-E KO mouse line by evaluating the expression of Siglecs-7 and -9 on TILs. Previous studies have shown that Siglecs-7 and -9 are expressed on TILs in a variety of human tumors (13). We assessed the expression of Siglecs-7 and 9 on TILs in Siglec-7/9/Siglec-E KO mice inoculated with B16 or MC38 solid tumors and observed that they are mostly expressed on infiltrating macrophages and neutrophils, and to a lesser extent on DCs, monocytes, NK cells, and T cells (Fig. 2*D* and *SI Appendix*, Fig. S2*A*). A recent study showed that Siglec-7 and Siglec-9 expression is elevated on peripheral blood T cells of cancer patients, compared to peripheral blood T cells of healthy donors (13). As in humans, we found that the Siglec-7/9/Siglec-E KO mouse line up-regulates Siglecs-7 and -9 on peripheral blood T cells of tumor-bearing mice, as compared to naïve mice (*SI Appendix*, Fig. S2 *B* and *C*). Importantly, the well-established murine tumor cell lines B16, MC38, EL4, and ID8 express ligands for either Siglec-7 or Siglec-9, which allowed us to use these syngeneic tumor models in our humanized murine model to evaluate the role of Siglec-7 and Siglec-9 in tumor progression (*SI Appendix*, Fig. S2*D*). Our data demonstrate that these mice recapitulate the expression pattern of the human Siglec-7 and Siglec-9 on peripheral blood mononuclear cells (PBMCs) as well as on TILs, and validate the use of this mouse line to study these two human receptors as therapeutic targets for immune therapy.

Siglec-E Absence Protects Mice from Tumor Challenge and Expression of Siglec-7 and Siglec-9 Reverses This Phenotype and Potentiates Tumor Growth. We next evaluated the impact of Siglec-E on tumor progression in several syngeneic mouse tumor models. We inoculated

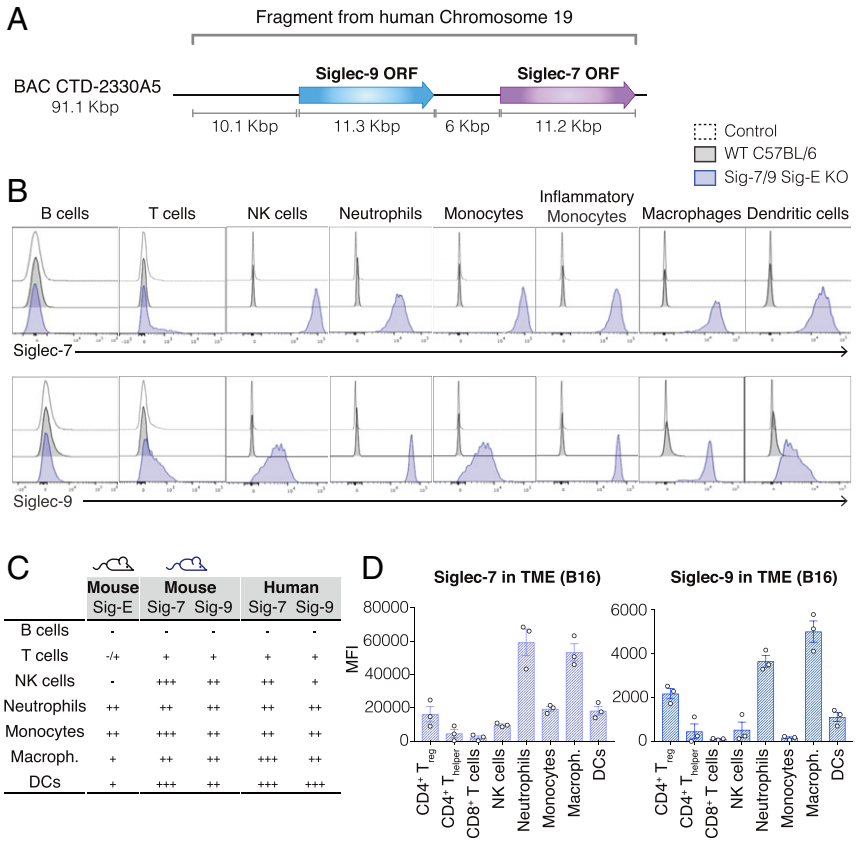

Fig. 2. Characterization of the Siglec-7/9/Siglec-E KO mouse model. (*A*) Generation of the Siglec-7/9/Siglec-E KO mouse strain: A BAC DNA fragment that contains the ORF of Siglec-7 and Siglec-9 and their regulatory elements was inserted into the genome of WT C57BL/6 mice to generate a mouse line expressing human Siglec-7 and Siglec-9 (Siglec-7/9 mice). This mouse line was then crossed to Siglec-E KO mice to generate the humanized Siglec-7/9/Siglec-E KO mouse line. (*B*) Surface expression of Siglec-7 (*Upper*) or Siglec-9 (*Lower*) on immune populations of WT C57BL/6 mice (black) or Siglec-7/9/Siglec-E KO mice (blue), compared to an unstained control (dashed line). Panel shows a representative mouse ($n > 9$). (*C*) Table summarizes expression patterns of Siglecs: Siglec-E on WT C57BL/6 mice (first column), Siglec-7 and Siglec-9 on Siglec-7/9/Siglec-E KO mice (*Center*) and Siglec-7 and Siglec-9 on human PBMCs (*Right*) based on MFI. (–, no expression; +, MFI brighter than control and $<10^4$; ++, MFI between 10^4 and 10^5; +++, MFI brighter than 10^5). (*D*) Expression of Siglec-7 (*Left*) or Siglec-9 (*Right*) on immune populations infiltrated into B16 solid tumors inoculated to Siglec-7/9/Siglec-E KO mice. Graph shows MFI of Siglec-7 or Siglec-9 as indicated, each circle represents one mouse. Data are displayed as mean ± SEM. Panel shows a representative experiment ($n = 2$).

WT C57BL/6 and Siglec-E KO mice with B16 (intravenously), B16 (subcutaneously), MC38 (subcutaneously), EL4 (intravenously), or ID8 (intraperitoneally) tumor cells and monitored tumor growth and survival. We found that there was no statistically significant difference in tumor growth or overall survival in most of the tumor models tested (*SI Appendix*, Fig. S3), which contrasts with previous studies (12). However, we observed a significant reduction in tumor burden in Siglec-E KO mice compared with WT C57BL/6 mice in the B16 lung colonization model. In this experimental setup, B16 cells are injected intravenously, lungs are excised 14 d postinoculation, and metastatic foci are quantified (Fig. 3 *A* and *B*). Overall, these findings indicate that Siglec-E has a more restricted impact on tumor progression than previously reported and that its influence is tissue specific. To investigate the role of Siglec-7 and Siglec-9 in tumor progression, we compared lung colonization in Siglec-7/9/Siglec-E KO mice to WT C57BL/6 and Siglec-E KO mice using the B16 lung metastasis model. Tumor burden in the lungs of Siglec-7/9/Siglec-E KO mice was increased compared to Siglec-E KO mice (although that increase did not reach statistical significance), and was comparable to that of WT C57BL/6 mice, suggesting that introducing Siglecs-7/9 can compensate for the absence of Siglec-E (Fig. 3 *A* and *B*).

To further dissect the role of Siglec-E in tumor progression and to determine the impact of tumor-expressed Siglec ligand density, we modified the B16 tumor line to increase the expression of ligands for Siglec-E, Siglec-7, and Siglec-9. Up-regulation of Siglec ligands is common during cancer progression, primarily in epithelial cancers refractory to immunotherapies (32). The carbohydrate Sialyl-Lewis A (sLeA) is a ligand of Siglec-E, Siglec-7, and Siglec-9 (*SI Appendix*, Fig. S4*A*), and its synthesis is partially catalyzed by the enzyme fucosyltransferase III (FUT3), which is not expressed in mice. We previously reported the development of a B16-FUT3 cell line, in which B16 cells were transduced to express human FUT3 and thereby sLeA (33). We inoculated WT C57BL/6, Siglec-E KO, and Siglec-7/9/Siglec-E KO mice with B16-FUT3 cells intravenously, and 14 d later evaluated lung colonization by counting lung metastatic foci. The number of metastatic foci in the lungs of Siglec-E KO mice was significantly reduced compared to WT C57BL/6 and to Siglec-7/9/Siglec-E KO mice (Fig. 3 *B* and *C*) and more pronounced with B16-FUT3 cells than with B16 cells, suggesting that elevated expression of Siglec ligands, such as sLeA, on tumor cells attenuates the antitumor immune response through interaction with Siglecs. To determine the generality of this observation, we compared tumor progression for two other sLeA-expressing tumor models: the lymphoma cell line EL4-FUT3 (33) and the pancreatic tumor cell line FC1242-FUT3-β3GalT5 (34). In contrast to the B16-FUT3 line, we did not observe a significant difference in survival or tumor growth between WT C57BL/6 mice and Siglec-E KO mice in either of the two tumor models (*SI Appendix*, Fig. S4*B*), again demonstrating that the contribution of Siglec-E is dictated by the tissue and specific TME.

The TME Dictates the Extent of Contribution of Siglec-E to Tumor Progression. In order to focus exclusively on how the difference in the tumor location and its anatomic microenvironment impact the role of Siglec-E on tumor progression, we implanted the same tumor cell line, B16-FUT3, through different routes: subcutaneously, intravenously, or through the spleen to induce subcutaneous solid tumors, lung tumors, or liver tumors, respectively. While the absence of Siglec-E leads to a significant reduction in tumor burden in the lung colonization model, it does not impact tumor growth when tumors are subcutaneous or in the liver (Fig. 3 *A*–*C* and *SI Appendix*, Fig. S5*A*). We hypothesized that different levels of Siglec-E expression on specific immune populations in the different tissues might contribute to the differential contribution of Siglec-E to tumor progression. Analysis of Siglec-E expression on TILs in the different tumor locations revealed that in subcutaneous and liver tumors, macrophages demonstrate the highest Siglec-E expression, while in lung tumors neutrophils show the highest Siglec-E levels (Fig. 3*D* and *SI Appendix*, Fig. S5*B*). Thus, the dominant expression of Siglec-E on macrophages in subcutaneous and liver tumors might reflect a more immunosuppressive—and thus less-responsive TME—than that of lung tumors. These data demonstrate that contribution of Siglec-E to inhibiting the antitumor immune response is highly dependent on its anatomic location and the specific cellular populations found in the TME.

Siglecs Inhibit the Response to Tumor-Targeting Antibodies. Since the absence of Siglec-E enhances the endogenous antitumor immune response in some tumors, we next examined its impact on response to tumor-targeting antibodies. We also investigated whether introducing Siglec-7 and Siglec-9 would be able to reverse any protective phenotype observed in Siglec-E KO mice. WT C57BL/6, Siglec-E KO, and Siglec-7/9/Siglec-E KO mice were inoculated subcutaneously with B16 cells (an experimental setup in which Siglec-E does not alter tumor development), and treated with either the antibody TA99, which targets the tumor antigen gp75 expressed on B16 cells, or with an isotype control (Fig. 3*E*). In control mice (treated with a mIgG2a isotype control), there was no statistically significant difference in tumor growth kinetics among the three mouse strains (WT C57BL/6, Siglec-E KO, or Siglec-7/9/Siglec-E KO). Similarly, we did not observe statistically significant differences in tumor growth kinetics between isotype-treated WT C57BL/6 mice and anti-gp75–treated WT C57BL/6 mice, or between isotype-treated Siglec-7/9/Siglec-E KO mice and anti-gp75–treated Siglec-7/9/Siglec-E KO mice. In contrast, Siglec-E KO mice treated with anti-gp75 developed significantly smaller tumors than Siglec-E KO mice treated with an isotype control, suggesting that Siglec-E dampens the response to tumor-targeting antibodies (Fig. 3 *E*–*G*). Taken together, our findings demonstrate in a fully congenic mouse background that Siglec-7 and Siglec-9, similarly to Siglec-E, can inhibit the endogenous antitumor immune response as well as the response to antibody therapy that targets tumor antigens.

Siglec-E Inhibits the Response to Checkpoint Therapy. Similarly to the PD-1 pathway, Siglec-E generates an inhibitory signal on immune cells upon engagement by tumor cells. While PD-1 is mostly expressed on $CD8^+$ T cells, Siglec-E is primarily expressed on myeloid cells. Therefore, we determined whether the absence of Siglec-E could synergize with T cell checkpoint blockade. WT and Siglec-E KO mice were inoculated subcutaneously with MC38 tumor cells and treated with an anti-CTLA4 antibody once tumors became palpable. While anti-CTLA4 treatment alone was not sufficient to significantly reduce tumor growth in WT C57BL/6 mice compared with isotype-treated WT C57BL/6 mice, the lack of Siglec-E increased the efficacy anti–CTLA-4 treatment, as Siglec-E KO mice treated with anti-CTLA4 developed significantly smaller tumors than isotype-treated Siglec-E KO mice (Fig. 4 *A* and *B*). Since MC38 tumors are highly sensitive to PD-1 blockade and are rejected when treated with anti–PD-1 antibodies, we used B16 and B16-FUT3 solid tumors to test the response of Siglec-E KO mice to PD-1 blockade. Once B16 or B16-FUT3 tumors are palpable, they are refractory to single-agent therapy (35, 36). However, we observed that combining anti–PD-1 with the tumor-targeting anti-gp75 antibody significantly reduced B16 tumor growth in WT C57BL/6 mice compared to isotype control-treated mice. Interestingly, Siglec-E KO mice demonstrated an even more robust response than WT C57BL/6 mice to combination therapy, with all Siglec-E KO mice showing significantly reduced tumor growth (Fig. 4 *C* and *D*). A similar effect was observed when mice were inoculated with cells that express higher levels of Siglec ligands, B16-FUT3 (Fig. 4*E*). Siglec-E KO mice that received a combination of anti–PD-1 and anti-sLeA antibodies developed significantly smaller tumors than isotype-treated Siglec-E KO mice. In contrast, WT C57BL6 mice did not respond to this treatment and developed tumors with similar growth kinetics as isotype-treated WT C57BL/6 mice (Fig. 4 *E* and

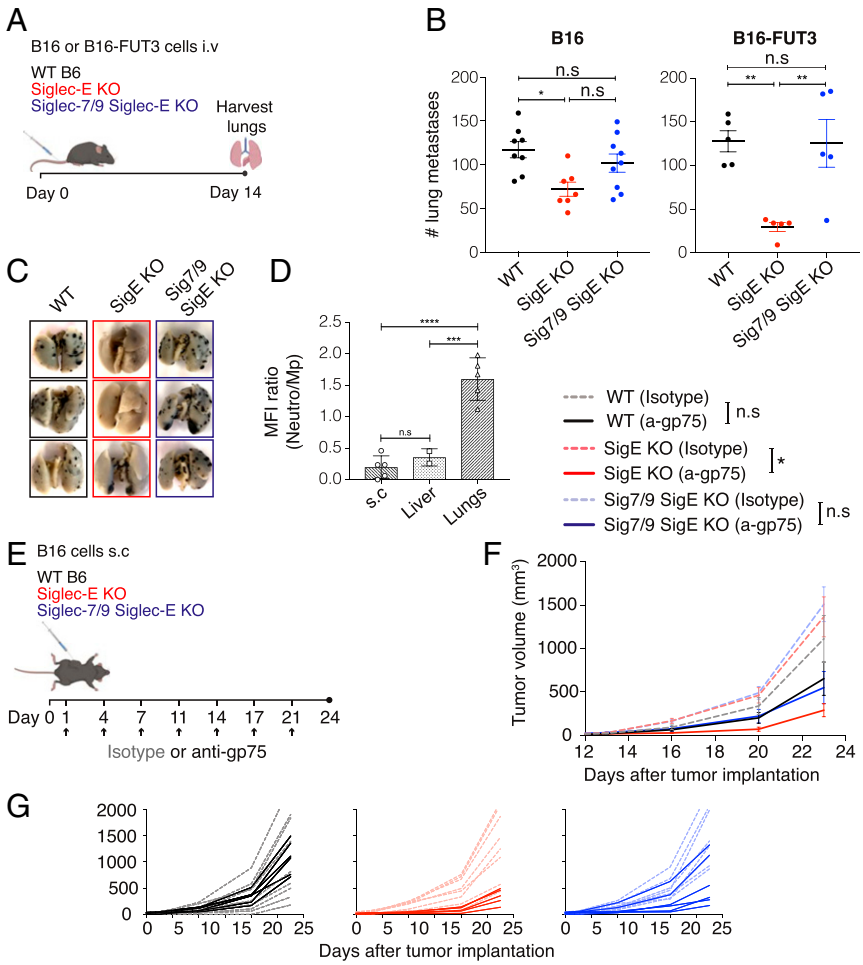

Fig. 3. Siglec-E absence protects mice from tumor challenge and expression of Siglec-7 and Siglec-9 reverses this phenotype and potentiates tumor growth. (*A*) Illustration of the experimental design. Mice were inoculated intravenously with 1×10^6 B16 cells or 0.5×10^6 B16-FUT3 cells. Fourteen days after inoculation, mice were killed, lungs were harvested and fixed, and metastatic foci were counted. (*B*) Number of B16 (*Left*) or B16-FUT3 (*Right*) metastatic foci in the lungs of WT C57BL/6 (black), Siglec-E KO (red) or Siglec-7/9/Siglec-E KO (blue) mice. Each circle represents an individual mouse. Graph shows a representative experiment ($n = 3$ experiments). Data are displayed as mean ± SEM. (*C*) Representative images of lungs excised from the indicated mouse strains 14 d postinoculation with B16-FUT3 cells. (*D*) Relative Siglec-E expression between neutrophils and macrophages in WT C57BL/6 mice, presented as Siglec-E MFI ratio in B16-FUT3 tumors located in different organs (subcutaneous, liver or lungs). (*E*) Illustration of the experimental design. Mice were inoculated subcutaneously (s.c.) with 0.2×10^6 B16 cells, and treated with 200 μg of anti-gp75 antibody or an isotype-matched control on the indicated days (arrow). Tumor volume was measured twice weekly using a digital caliper. (*F*) Tumor growth of B16 cells in WT C57BL/6 (black), Siglec-E KO (red), or Siglec7/9/Siglec-E KO mice (blue). Solid lines represent groups treated with anti-gp75 antibody, while dashed faint lines represent groups treated with an isotype control. Average sizes of primary tumors ± SEM are presented in cubic millimeters (mm^3; $n = 5$ to 9 mice per group). (*G*) Tumor growth curves of individual mice from (*F*). $^*P < 0.05$; $^{**}P < 0.01$; $^{***}P < 0.005$; $^{****}P < 0.0001$; ns, nonsignificant (one-way ANOVA).

F). Collectively, these results indicate that targeting Siglec-E can synergize with checkpoint blockade to enhance antitumor responses.

Siglec-7– and Siglec-9–Targeting Antibodies Reduce Tumor Burden. Having determined that perturbation of Siglec-E could augment antitumor immunotherapy, we next assessed whether antibodies blocking Siglecs-7 and -9 can be used to reduce tumor burden. We selected anti–Siglec-7 and anti–Siglec-9 antibodies previously demonstrated to efficiently block these receptors (37, 38) and modified their Fc regions to prevent engagement of Fcγ receptors (FcγRs) and thus reduce the likelihood of depletion of Siglec-expressing immune cells. The variable region of each antibody was cloned into a mouse IgG1-D265A Fc backbone, which lacks detectable FcγR binding (39). To confirm that the Fc engineered and expressed antibodies retain their blocking activity, we analyzed the binding of soluble Siglec-7 or Siglec-9 to B16-FUT3 cells in the presence of increasing concentrations of each of the candidate antibodies (Fig. 5*A*). Antibody clones 1E8 (anti–Siglec-7) and mAbA (anti–Siglec-9) were selected based on their ability to block Siglecs-7/9 from binding to B16-FUT3 cells (Fig. 5*B*).

We next evaluated the effect of the two blocking antibodies on tumor progression in the B16-FUT3 lung colonization model. Siglec-7/9/Siglec-E KO were inoculated intravenously with B16-FUT3 cells and treated with either a combination of anti–Siglec-7 and anti–Siglec-9 antibodies or with isotype-matched control antibodies. Fourteen days after tumor cell inoculation, lungs were harvested and assessed for presence of surface metastatic foci (Fig. 5*C*). Siglec-7/9/Siglec-E KO mice that received anti–Siglec-7 and anti–Siglec-9 antibodies showed significantly lower tumor burden than mice that received isotype-control antibodies, although the reduction in tumor burden did not reach the low number of metastatic foci observed in Siglec-E KO mice that served as control. (Fig. 5*D*). Altogether, our data show that targeting the human Siglec-7 and Siglec-9 with blocking antibodies is a promising

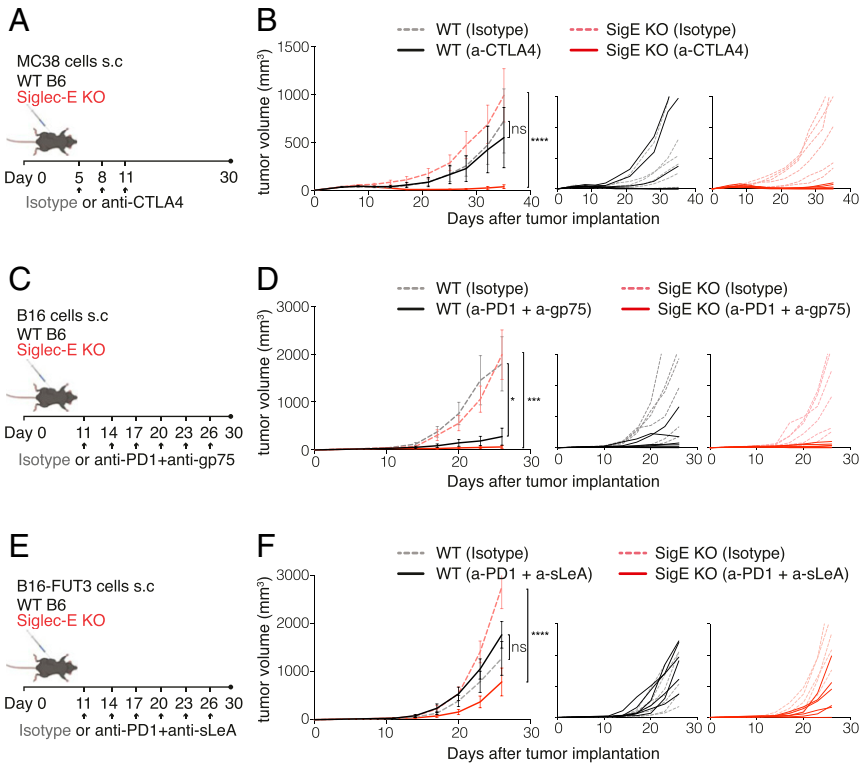

Fig. 4. Siglec-E inhibits the response to checkpoint therapy. (*A*, *C*, and *E*) Illustration of the experimental design. WT C57BL/6 mice (black) or Siglec-E KO mice (red) were inoculated with 2×10^6 MC38 (*A* and *B*), 0.2×10^6 B16 (*C* and *D*), or 0.2×10^6 B16-FUT3 (*E* and *F*) tumor cells. Once tumors reached a volume larger than 30 mm^3, mice were treated with an anti-CTLA4 antibody (*A* and *B*), a combination of anti–PD-1 + anti-gp75 antibodies (*C* and *D*), a combination of anti–PD-1 + anti-sLeA antibodies (*E* and *F*), or with an isotype-matched control. Two hundred micrograms of each antibody were inoculated intraperitoneally every 3 d after treatment onset (arrows). Tumor volume was measured twice weekly using a digital caliper. (*B*, *D*, and *F*, *Left*) Tumor growth of MC38, B16, and B16-FUT3 cells, respectively, in WT C57BL/6 (black) or Siglec-E KO (red) mice. Solid lines represent groups treated with the indicated therapeutic antibodies, while dashed faint lines represent groups treated with an isotype control. Average sizes of primary tumors ± SEM are presented in cubic millimeters (mm^3) (n = 6 to 7 mice per group). (*B*, *D*, and *F*, *Right*) Tumor growth curves of individual mice from for each tumor model. *$P < 0.05$; **$P < 0.01$; ***$P < 0.005$; ****$P < 0.0001$; ns, nonsignificant (one-way ANOVA). Tumor volumes are shown in cubic millimeters (mm^3).

strategy to enhance antitumor immunity and reduce tumor burden (Fig. 6).

Discussion

The emergence of ICIs has been a major milestone for cancer treatment. The groundbreaking success of this type of therapy highlights the therapeutic potential of targeting immune modulators to treat cancer. However, the limited efficacy of these treatments for the majority of patients indicates the large unmet need for novel therapeutics targeting immune regulatory pathways and highlights the necessity to develop new strategies to manipulate them. The family of Siglec receptors represents a promising route to further release the brakes of the immune system beyond targeting the PD-1/PD-L1 and CTLA4 pathways. Here, we describe the role of Siglec-7 and Siglec-9 in tumor progression and propose to use these receptors as immune modulatory targets for cancer therapy. Our studies were facilitated through the use of a mouse model that recapitulates the expression pattern of Siglec-7 and Siglec-9 in humans while lacking expression of the murine counterpart, Siglec-E, on a syngenic C57BL/6 background.

Previous in vivo studies on the impact of Siglec-9 and its murine homolog Siglec-E on tumor progression have relied on the use of mixed background murine models and have generated contradictory results (12). Based on these studies, it was proposed that Siglec-E and Siglec-9 have a dualistic function: inhibiting immune response during early tumorigenesis, while promoting antitumor immunity once tumors are established. However, the authors used a Siglec-E KO mouse model that was generated in a 129/Sv background and then backcrossed to a C57BL/6 background, which might explain this confounding result. By using mouse models generated in a fully C57BL/6 background, we were able to show that their impact on tumor progression is more dependent on the anatomic site of the tumor and its immediate TME than previously described. In contrast to these prior studies, we did not observe a significant difference in tumor progression between WT and Siglec-E KO mice in all solid tumor models tested, including B16 and MC38, as well as in lymphoma and ovarian tumor models. However, Siglec-E KO mice did exhibit reduced tumor burden in a B16 lung colonization model compared to WT mice, and expression of Siglec-7 and Siglec-9 reversed this protective phenotype. Increasing the density of Siglec ligands on the surface of B16 cells (B16-FUT3) increased the tumorigenic potential of these cells (33) and also made them more sensitive to absence of Siglec-E. This supports the hypothesis that these tumor cells are able to evade immune attack by engaging Siglecs on immune cells.

Despite the enhanced phenotype observed in the B16-FUT3 lung colonization experimental setup, most of the tumor models that we tested were not sensitive to the deletion of Siglec-E, including the tumor cell lines EL4-FUT3 and FC1242-FUT3-β3GalT5 that also have higher expression of the Siglec-E ligand sLeA. These findings suggest that not only the density of Siglec ligands on tumor cells, but also the anatomical location of the tumor and therefore the TME dictate the contribution of Siglecs to tumor development. Comparison of Siglec-E expression levels between tumors that are sensitive and tumors that are refractory to lack of Siglec-E revealed that the latter show predominant Siglec-E expression

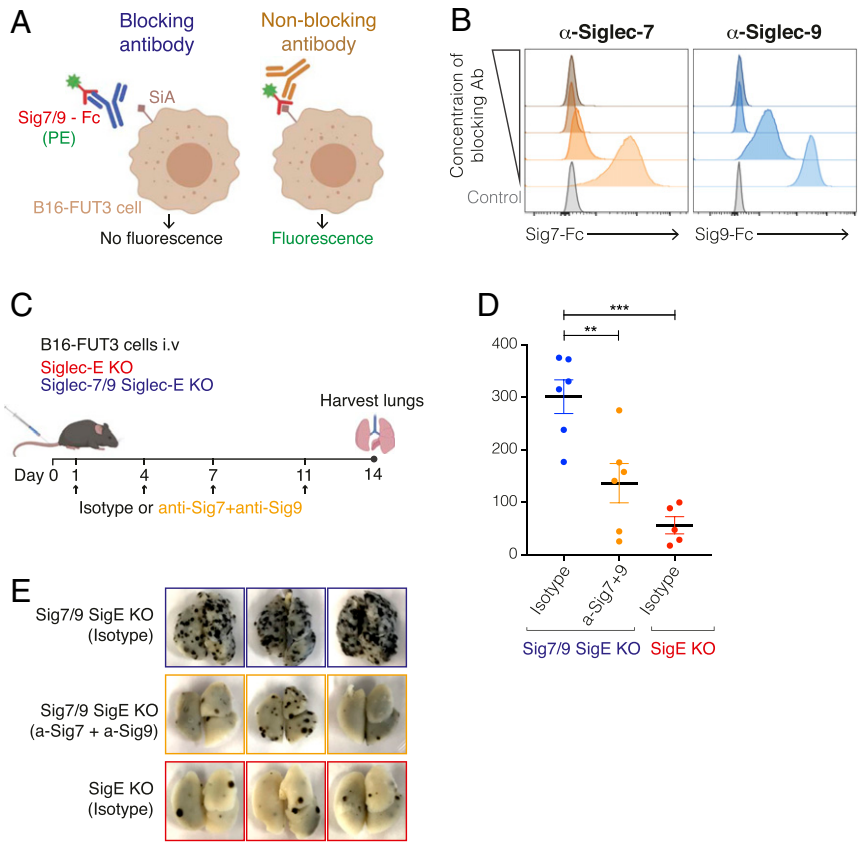

Fig. 5. Siglec-7– and Siglec-9–targeting antibodies reduce tumor burden in mice. (*A*) Illustration of the experimental design to evaluate the blocking ability of different Siglec-7 and Siglec-9 antibody clones. Siglec-7–Fc or Siglec-9–Fc chimeras (hIgG) were preincubated with anti–Siglec-7 or anti–Siglec-9 antibodies (with a mIgG1 D265A Fc), respectively, followed by incubation with B16-FUT3 cells (that express high density of Siglec ligands, SiA). Binding of Siglecs to tumor cells was detected by a fluorescently labeled anti-human IgG antibody that bound to the Fc of the Siglec-Fc chimeras. (*B*) Binding of Siglec-7–Fc (*Left*) or Siglec-9–Fc (*Right*) chimeras to B16-FUT3 cells in the presence of increasing concentrations of anti–Siglec-7 (*Left*) or anti–Siglec-9 (*Right*) antibodies. (*C*) Illustration of experimental design. Mice were inoculated intravenously with B16-FUT3 cells and treated with a combination of anti–Siglec-7 + anti–Siglec-9 antibodies or an isotype-matched control on days 1, 4, 7, and 11 (arrows). On day 14 mice were killed, lungs were excised and fixed, and the number of lung metastatic foci was counted. (*D*) Number of B16-FUT3 metastatic foci in the lungs of Siglec-7/9/Siglec-E KO mice that received an isotype control (blue), or a combination of anti–Siglec-7 + anti–Siglec-9 antibodies (orange). Siglec-E KO mice that received an isotype control (red) served as control. Each circle represents an individual mouse. Graph shows a representative experiment ($n = 2$ experiments). Data are displayed as mean ± SEM $^{**}P < 0.01$; $^{***}P < 0.005$ (one-way ANOVA). (*E*) Representative images of lungs excised from the indicated mouse groups 14 d postinoculation with B16-FUT3 cells.

on macrophages, while in the former neutrophils are the immune population with the highest Siglec-E expression. The higher expression of Siglec-E on macrophages might reflect a more immunosuppressive TME, where additional tumor-promoting factors compensate for the lack of Siglec-E. Like macrophages, neutrophils can have antitumor or protumor functions. In the context of the lung, previous studies have showed that neutrophils can have an antitumor effect by inhibiting lung colonization (40). However, in vitro studies suggest that neutrophil activation and thus antitumor activity can be inhibited by engagement of Siglec-9 by sialylated tumor-associated ligands (12). Thus, lack of Siglec-E, Siglec-7, and Siglec-9 expression in our mouse model might allow enhanced neutrophil activation and thus protective activity against lung colonization. For tumor models where Siglec-E did not significantly affect tumor growth, we did find that the absence of Siglec-E allowed for a more robust response to tumor-targeting and checkpoint-targeting antibodies. Altogether, these data indicate that targeting Siglecs, either alone or in combination with other antibody therapies, represents a promising strategy to increase antitumor immunity.

Antibodies targeting Siglecs have traditionally been designed to deplete specific immune cells and thereby treat certain conditions. For example, Inotuzumab (anti–Siglec-2) for B cell acute lymphocytic leukemia, Gemtuzumab (anti–Siglec-3) for acute myeloid leukemia, and Lirentelimab (anti–Siglec-8) for eosinophilic gastritis (41, 42). However, the use of anti-Siglec antibodies to modulate the response of immune cells rather than depleting them, is a therapeutic strategy deserving of further investigation. Currently, just one such antibody is being evaluated in clinical trials, an anti–Siglec-15 antibody (NC318) that reverses T cell suppression by blocking the interaction between macrophages and T cells (14). Similarly, there are several preclinical studies on blocking Siglec-7 and Siglec-9 antibodies that have shown promising in vitro data (37, 38, 43). However, the lack of mouse models that faithfully recapitulate the human expression patterns of Siglec-7 and Siglec-9, while lacking expression of the mouse homolog Siglec-E, has hindered progress on evaluating the antitumor effect of these antibodies in vivo. Here, we developed a Siglec-7/9/Siglec-E KO mouse model that allows testing the therapeutic potential of anti–Sigec-7– and anti–Siglec-9–targeting antibodies. We screened several anti–Siglec-7 and anti–Siglec-9 antibody clones for their ability to block the interaction between Siglecs-7 and -9 and their ligands on tumor cells, and selected the clones with the highest blocking activity. Both the Fab and the Fc portion of an antibody contribute to its blocking activity: the former by preventing interaction of the receptor with its ligand, and the latter by preventing engagement of effector cells through their FcγRs. Therefore,

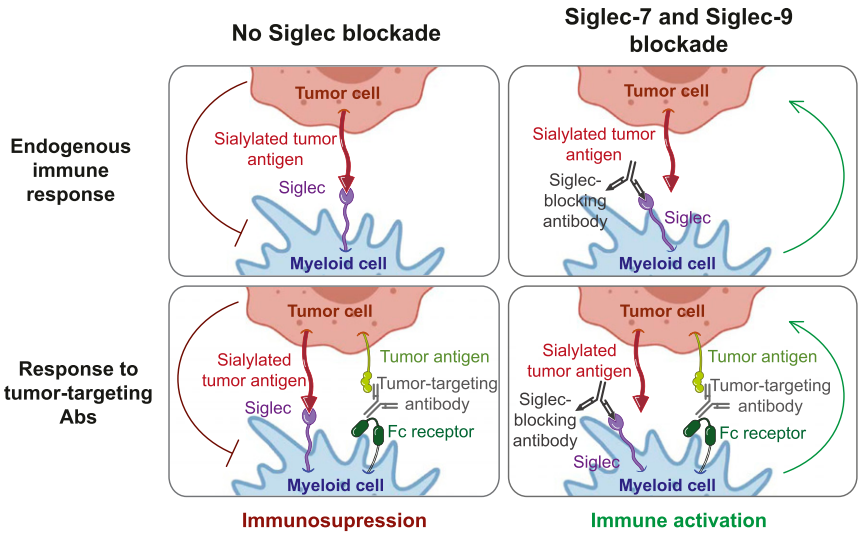

Fig. 6. Proposed model. Siglec-7 and Siglec-9 can inhibit the endogenous antitumor immune response as well as the response to tumor-targeting and checkpoint-targeting antibodies. Blockade of Siglec-7 and Siglec-9 releases this inhibition and enhances antitumor immunity.

we engineered both Siglec-7 and Siglec-9 antibodies to block FcγRs binding by introducing a point mutation in their Fc region. By using these engineered antibodies, we were able to significantly reduce tumor burden in Siglec-7/9/Siglec-E KO mice. Previous in vitro studies have shown that engagement of Siglec-9 by a cancer-specific mucin induces a tumor-associated macrophage (TAM) phenotype on Siglec-9–expressing macrophages, and that this phenotypic change can be rescued by blockade of Siglec-9 (26). Together with our in vivo data, this suggests that anti–Siglec-7 and Siglec-9 antibodies function by preventing polarization of macrophages into TAMs and thus reprogramming the immune-suppressive TME. However, it does not rule out the possibility that other immune populations are also involved in the therapeutic antitumor activity of these antibodies. Altogether, our findings show that Siglec-7 and Siglec-9 can inhibit the antitumor immune response and demonstrate that targeting these human Siglecs is a promising therapeutic strategy to enhance antitumor immunity.

Materials and Methods

Mice. WT C57BL/6 mice were purchased from The Jackson Laboratories. All studies were performed on 8- to 12-wk old age- and sex-matched female and male mice. All in vivo experiments were performed in compliance with federal laws and institutional guidelines and have been approved by The Rockefeller University Institutional Animal Care and Use Committee. Transgenic mice were bred and maintained at the Comparative Bioscience Center at The Rockefeller University.

Generation of Siglec-E KO Mice. To create Siglec-E KO mice, several CRISPR guides were designed targeting exons 2 and 3. Based on testing in mouse embryonic stem cells, a CRISPR target sequence was identified on exon 3 (TGAGTCAGCTCCTTGATAGATGG; PAM underlined) that yielded optimal cleavage efficiency with the desired frame shift mutation pattern by the Cas9 endonuclease (Rockefeller University Gene Targeting Facility). This guide was subsequently delivered as a RNP complex (crRNA+tracrRNA+Cas9 protein) into mouse zygote via zygote injection. G0 mice were screened by DNA sequence and two separate genetic mutations were identified, a 4-bp and an 11-bp deletion, both resulting in a frame shift creating an early termination codon after amino acid 249 of the protein. Individual mutant founders (G0) were subsequently crossed to C57BL/6 mice and the G1 progeny were screened to identify presence of individual genetic events. For ease of PCR screening, we chose to use the mouse line containing only the 11-bp deletion and conducted characterization experiments screening for lack of Siglec-E expression. Siglec-E KO mice were maintained on the C57BL/6 genetic background.

Generation of Siglec-7/9 Siglec-E KO Transgenic Mice. Transgenic mice carrying both the human transgenes for SIGLEC7 and SIGLEC9 were made using a genomic DNA isolated from a human blood DNA library (CTD-2330A5, CalTech BAC library D; Thermofisher). The linearized BAC DNA was microinjected into the pronuclei of fertilized oocytes from C57BL/6 mice. Transgenic founders were then crossed and maintained on C57BL/6 mouse background to propagate the line and analyzed for correct tissue expression of the Siglec-7 and Siglec-9 proteins. The Siglec-7/9 mice were then mated with Siglec-E KO mice to obtain Siglec-7/9 Siglec-E KO mice.

Cell Lines. B16F10, MC38, ID8, and EL4 cells were obtained from ATCC. FC1242-FUT3, β3GalT5 cells were provided by Danielle Engle, Salk Institute for Biological Studies, San Diego, CA, and from David Tuveson, Cold Spring Harbor Laboratory, Cold Spring Harbor, NY. B16-FUT3 and EL4-FUT3 cells were generated as previously described (33). All cell lines were maintained in Dulbecco's minimum essential medium (Life Technologies) supplemented with 10% fetal bovine serum (Life Technologies), 100 U/mL of penicillin, and 100 μg/mL of streptomycin (Life Technologies).

Antibody Engineering and Expression. The variable heavy and light regions of anti–Siglec-7 (clone 1E8) and anti–Siglec-9 (clone mAbA) antibodies (described in patents WO/2017/040301Al, and WO/2017/153433Al, respectively) were synthesized (IDT) and subcloned into mammalian expression vectors with a mouse IgG1 heavy chain containing a D265A point mutation, or a mouse κ-light chain, as previously described (33, 44). Expression plasmids for anti–PD-1 (clone RMP1-14, mIgG1 D265A) and anti-sLeA (clone 5B1, mIgG2a) antibodies were previously generated in the laboratory (33, 45). Plasmid sequences were validated by direct sequencing (Genewiz).

Expi293F cells were used to generate antibodies. Briefly, Expi293F cells were maintained in Expi293 Expression Medium (Thermo Fisher Scientific, cat# A1435101), and transfected with heavy-chain and light-chain constructs using an ExpiFectamine 293 Transfection Kit (Thermo Fisher Scientific, cat# A14525). Seven days after transfection, supernatants were collected, centrifuged, and filtered. Clarified supernatants were incubated with Protein G Sepharose 4 Fast Flow (GE Healthcare) overnight. The next day Protein G beads were washed with PBS, bound antibodies were eluted using IgG elution buffer (Thermo Fisher Scientific, cat# 21009), dialyzed in PBS, and sterile-filtered, as previously described (33, 46). Anti-gp75 (clone TA99) and anti–CTLA-4 (clone UC10-4F10-11) antibodies were purchased from BioXCell (cat# BE0151 and BE0032, respectively).

Tissue Processing and Flow Cytometry.

Surface expression of Siglec ligands on murine tumor cell lines. Expression was assessed using Fc chimeras of Siglec-E, Siglec-7, or Siglec-9 (R&D Systems, cat# 5806-SL-050, 1138-SL-050, and 1139-SL-050, respectively). Tumor cells (1×10^6) were incubated with 1 μg of Fc-Siglec fusion protein, followed by R-Phycoerythrin–conjugated secondary antibodies against mouse IgG for

Siglec-E-Fc (Jackson ImmunoResearch cat# 715-116-151), or against human IgG for Siglec-7-Fc and Siglec-9-Fc (Jackson ImmunoResearch cat# 709-116-149). Baseline staining was obtained using PBS followed by the fluorescently labeled secondary antibody.

Characterization of Siglec-E, Siglec-7, or Siglec-9 expression in transgenic mice. Peripheral blood (for T cell, B cell, NK cell, neutrophil, and monocyte staining), spleen (for DC staining), and bone marrow cells (for macrophage staining) were collected. Spleens were homogenized by mechanical shearing and passed through a 70-μm strainer (Corning) to obtain a single-cell suspension. For intratumoral analysis, subcutaneous tumors were surgically resected, and processed using a tumor dissociation Kit (Miltenyi Biotec). For analysis of lung and liver tumors, lungs and livers were harvested and processed using a lung dissociation kit and a liver dissociation kit, respectively, following the manufacturer's instructions (Miltenyi Biotec). After lysis of red blood cells (RBC lysis buffer; BioLegend), single-cell suspensions were labeled with the LIVE/DEAD Fixable Aqua (ThermoFisher) and resuspended in PBS containing 0.5% (wt/vol) BSA and 5 mM EDTA. Cells were then stained with antibodies against surface markers. FoxP3 staining was performed using the FOXP3 Fix/Perm buffer set (BioLegend) following the manufacturer's instructions.

Characterization of Siglec-7 or Siglec-9 expression in humans. Leukocyte packs (buffy coats) were purchased from the New York Blood Center and mononuclear cells or neutrophils were isolated by Ficoll gradient centrifugation. $CD14^+$ monocytes were purified using CD14 microbeads (Miltenyi Biotech) and subsequently incubated with 100 ng/mL granulocyte-macrophage colony-stimulating factor and 100 ng/mL interleukin-4 to differentiate them into DCs. To isolate macrophages, PBMCs were allowed to adhere to a Petri dish and unbound cells were washed off with PBS. Macrophages attached to the Petri dish were stained 6 d postisolation. Cell populations were defined by the following markers: T cells (human: $CD3^+$; mouse $CD3^+$), $CD4^+$ T_{regs} (mouse $CD3^+CD4^+CD8^-FoxP3^+$), $CD4^+$ T_{helper} (mouse $CD3^+CD4^+CD8^-FoxP3^-$), B cells (human: $CD19^+$; mouse: $CD19^+$), NK cells (human: $CD16^+CD56^+CD3^-$; mouse: $NK1.1^+$), neutrophils (human: $CD16^+$; mouse: $CD11b^+Gr1^+SSC^{high}F4/80^-$), monocytes (human: $CD14^+CD16^{+/-}$; mouse: $CD11b^+Gr1^-F4/80^-CD11c^-$), macrophages (human: $CD14^+CD68^+$; mouse: $CD11b^+F4/80^+MHCII^+$), and DCs (human $HLA\text{-}DR^+BDCA1^+CD209^+CD3^-CD14^-CD19^-CD59^-$; mouse: $CD11b^+CD11c^+MHCII^+F4/80^-$). Samples were collected on an Attune NxT flow cytometer (ThermoFisher) using Attune NxT software v3.1.2 and analyzed using FlowJo (v10.6) software.

Tumor Challenge and Antibody Treatments. For the B16 and B16-FUT3 lung colonization models 1×10^6 cells or 0.5×10^6 cells per mouse, respectively, were inoculated intravenously into the lateral tail vein in 200 μL PBS. Mice were randomized and for the B16-FUT3 model mice received intraperitoneal injections of 200 μg of anti–Siglec-7 and 200 μg of anti–Siglec-9 antibodies or isotype-matched IgGs on days 1, 4, 7, and 11 after tumor inoculation. On day 14 lungs were harvested and analyzed for the presence of surface metastatic foci using a dissecting microscope. For the B16 and B16-FUT3 solid tumor models, 0.2×10^6 cells per mouse were inoculated subcutaneously and tumor volumes were measured biweekly using an electronic caliper. Tumor volumes are reported as volume (mm^3) and were calculated using the formula $(L1^2 \times L2)/2$, where L1 is the shortest diameter and L2 is the longest diameter (33). For treatment with anti-gp75, mice received intraperitoneal injections of 200 μg of antibody every 3 d starting on day 1 after tumor implantation. Nonengrafted tumors were removed from the quantification. For treatment with either anti-gp75 + anti–PD-1, or anti-gp75 + anti-sLeA, once tumors reached a volume larger than 30 mm^3 mice received intraperitoneal injections of 200 μg of each antibody. For the B16-FUT3 liver metastasis model, 0.5×10^6 cells per mouse were inoculated into the spleen, and the spleen was subsequently removed. Livers were harvested on day 12 and analyzed for the presence of surface metastatic foci using a dissecting microscope. For the EL4 and EL4-FUT3 lymphoma models, 0.5×10^6 cells per mouse were inoculated intravenously into the lateral tail vein in 200 μL PBS and overall survival was assessed daily. For the MC38 solid tumor model, 2×10^6 cells per mouse were inoculated subcutaneously and tumor volumes were measured biweekly using an electronic caliper. Once tumors reached a volume larger than 30 mm^3, mice were randomized and received intraperitoneal injections of 200 μg of anti–CTLA-4 or isotype-matched IgGs. For the ID8 ovarian tumor model 10×10^6 cells per mouse were inoculated intraperitoneally and survival was assessed daily. For the FC1242-FUT3-β3GalT5 solid tumor model 0.1×10^6 cells per mouse were inoculated subcutaneously and tumor volumes were measured biweekly using an electronic caliper.

ELISA. Binding of Siglec-E, Siglec-7, or Siglec-9 to sLeA (CA19-9) was detected by ELISA. High-binding 96-well microtiter plates (Nunc) were coated with 100 U of sLeA (Biorbyt Cat# orb82223) and incubated overnight at 4 °C. The next day plates were blocked for 1 h with PBS/2% chicken albumin (Sigma cat# A5503) and then incubated for 1 h with serially diluted Fc chimeras of Siglec-E, Siglec-7, or Siglec-9 (R&D Systems). Fc chimeras of CD19 (mouse IgG, 9730-CD-050) or CTLA-4 (human IgG, R&D Systems cat# 434-CT/CF) were used as negative controls. Finally, plates were incubated for 1 h with HRP-conjugated anti-mouse IgG or anti-human IgG antibodies (Jackson ImmunoResearch cat# 115-035-146, or cat# 109-035-088, respectively). Detection was performed using a TMB Peroxidase Substrate Kit (SeraCare, cat# 50-76-00) and reactions stopped with the addition of 2 M phosphoric acid. Absorbance was measured at 450 nm using a SpectraMax Plus spectrophotometer (Molecular Devices). Background absorbance of negative controls was subtracted from experimental samples and duplicate wells were then averaged (33).

Statistics. An unpaired two-tailed *t* test was used when two groups were being compared. One-way ANOVA with Bonferroni's post hoc test was used when more than two groups were compared. For survival rates, statistical differences between groups were analyzed by comparing Kaplan–Meier curves using the log-rank test (33). GraphPad Prism software was used for all statistical analysis. *P* values of ≤ 0.05 were considered to be statistically significant (indicated as $^*P \leq 0.05$, $^{**}P \leq 0.01$, $^{***}P \leq 0.001$, and $^{***}P \leq 0.0001$).

Data Availability. All study data are included in the article and *SI Appendix*.

ACKNOWLEDGMENTS. We thank D. Knorr for fruitful discussions and for reviewing the manuscript; J. Osorio for reviewing the manuscript and for help with the liver metastasis tumor model; H. Smith, H. Tector, R. Peraza, and E. Lam for excellent technical assistance; all the members of the J.V.R. laboratory for helpful discussions; Dannielle Engle (Salk Institute for Biological Studies) and David Tuveson (Cold Spring Harbor Laboratory) for generously providing the FC1242-FUT3,β3GalT5 cell line; and The Rockefeller University for continued institutional support and its available resources. Research reported in this publication was supported by the National Cancer Institute of the NIH under Awards R35CA196620 and R01CA244327. This research was supported in part by The Kimberly Lawrence-Netter Cancer Research Discovery Fund at The Rockefeller University (I.I.-B.). The content is solely the responsibility of the authors and does not necessarily represent the official views of the NIH.

1. D. R. Leach, M. F. Krummel, J. P. Allison, Enhancement of antitumor immunity by CTLA-4 blockade. *Science* **271**, 1734–1736 (1996).
2. G. J. Freeman *et al*., Engagement of the PD-1 immunoinhibitory receptor by a novel B7 family member leads to negative regulation of lymphocyte activation. *J. Exp. Med.* **192**, 1027–1034 (2000).
3. H. Dong, G. Zhu, K. Tamada, L. Chen, B7-H1, a third member of the B7 family, co-stimulates T-cell proliferation and interleukin-10 secretion. *Nat. Med.* **5**, 1365–1369 (1999).
4. R. K. Vaddepally, P. Kharel, R. Pandey, R. Garje, A. B. Chandra, Review of indications of FDA-approved immune checkpoint inhibitors per NCCN guidelines with the level of evidence. *Cancers (Basel)* **12**, 738 (2020).
5. P. Sharma, S. Hu-Lieskovan, J. A. Wargo, A. Ribas, Primary, adaptive, and acquired resistance to cancer immunotherapy. *Cell* **168**, 707–723 (2017).
6. J. S. O'Donnell, G. V. Long, R. A. Scolyer, M. W. Teng, M. J. Smyth, Resistance to PD1/PDL1 checkpoint inhibition. *Cancer Treat. Rev.* **52**, 71–81 (2017).
7. A. M. Georgoudaki *et al*., Reprogramming tumor-associated macrophages by antibody targeting inhibits cancer progression and metastasis. *Cell Rep.* **15**, 2000–2011 (2016).
8. S. Eisinger *et al*., Targeting a scavenger receptor on tumor-associated macrophages activates tumor cell killing by natural killer cells. *Proc. Natl. Acad. Sci. U.S.A.* **117**, 32005–32016 (2020).
9. M. K. Srivastava *et al*., Myeloid suppressor cell depletion augments antitumor activity in lung cancer. *PLoS One* **7**, e40677 (2012).
10. D. G. DeNardo *et al*., Leukocyte complexity predicts breast cancer survival and functionally regulates response to chemotherapy. *Cancer Discov.* **1**, 54–67 (2011).
11. S. B. Coffelt *et al*., IL-17-producing γδ T cells and neutrophils conspire to promote breast cancer metastasis. *Nature* **522**, 345–348 (2015).
12. H. Läubli *et al*., Engagement of myelomonocytic Siglecs by tumor-associated ligands modulates the innate immune response to cancer. *Proc. Natl. Acad. Sci. U.S.A.* **111**, 14211–14216 (2014).
13. M. A. Stanczak *et al*., Self-associated molecular patterns mediate cancer immune evasion by engaging Siglecs on T cells. *J. Clin. Invest.* **128**, 4912–4923 (2018).
14. J. Wang *et al*., Siglec-15 as an immune suppressor and potential target for normalization cancer immunotherapy. *Nat. Med.* **25**, 656–666 (2019).
15. A. A. Barkal *et al*., CD24 signalling through macrophage Siglec-10 is a target for cancer immunotherapy. *Nature* **572**, 392–396 (2019).
16. C. Büll *et al*., Sialic acid blockade suppresses tumor growth by enhancing T-cell-mediated tumor immunity. *Cancer Res.* **78**, 3574–3588 (2018).
17. P. R. Crocker, J. C. Paulson, A. Varki, Siglecs and their roles in the immune system. *Nat. Rev. Immunol.* **7**, 255–266 (2007).
18. J. C. Paulson, M. S. Macauley, N. Kawasaki, Siglecs as sensors of self in innate and adaptive immune responses. *Ann. N. Y. Acad. Sci.* **1253**, 37–48 (2012).

19. L. Cassetta *et al*., Human tumor-associated macrophage and monocyte transcriptional landscapes reveal cancer-specific reprogramming, biomarkers, and therapeutic targets. *Cancer Cell* **35**, 588–602.e10 (2019).
20. A. Varki *et al*., *Essentials of Glycobiology* (Cold Spring Harbor Laboratory Press, 2015).
21. B. H. Sanford, An alteration in tumor histocompatibility induced by neuraminidase. *Transplantation* **5**, 1273–1279 (1967).
22. M. S. Macauley, P. R. Crocker, J. C. Paulson, Siglec-mediated regulation of immune cell function in disease. *Nat. Rev. Immunol.* **14**, 653–666 (2014).
23. H. Cao *et al*., Comparative genomics indicates the mammalian CD33rSiglec locus evolved by an ancient large-scale inverse duplication and suggests all Siglecs share a common ancestral region. *Immunogenetics* **61**, 401–417 (2009).
24. C. Jandus *et al*., Interactions between Siglec-7/9 receptors and ligands influence NK cell-dependent tumor immunosurveillance. *J. Clin. Invest.* **124**, 1810–1820 (2014).
25. Q. Haas *et al*., Siglec-9 regulates an effector memory $CD8^+$ T-cell subset that congregates in the melanoma tumor microenvironment. *Cancer Immunol. Res.* **7**, 707–718 (2019).
26. R. Beatson *et al*., The mucin MUC1 modulates the tumor immunological microenvironment through engagement of the lectin Siglec-9. *Nat. Immunol.* **17**, 1273–1281 (2016).
27. J. E. Hudak, S. M. Canham, C. R. Bertozzi, Glycocalyx engineering reveals a Siglec-based mechanism for NK cell immunoevasion. *Nat. Chem. Biol.* **10**, 69–75 (2014).
28. M. Ohta *et al*., Immunomodulation of monocyte-derived dendritic cells through ligation of tumor-produced mucins to Siglec-9. *Biochem. Biophys. Res. Commun.* **402**, 663–669 (2010).
29. Y. Zheng *et al*., The roles of Siglec7 and Siglec9 on natural killer cells in virus infection and tumour progression. *J. Immunol. Res.* **2020**, 6243819 (2020).
30. S. von Gunten *et al*., Siglec-9 transduces apoptotic and nonapoptotic death signals into neutrophils depending on the proinflammatory cytokine environment. *Blood* **106**, 1423–1431 (2005).
31. H. Läubli *et al*., Lectin galactoside-binding soluble 3 binding protein (LGALS3BP) is a tumor-associated immunomodulatory ligand for CD33-related Siglecs. *J. Biol. Chem.* **289**, 33481–33491 (2014).
32. O. M. Pearce, H. Läubli, Sialic acids in cancer biology and immunity. *Glycobiology* **26**, 111–128 (2016).
33. P. Weitzenfeld, S. Bournazos, J. V. Ravetch, Antibodies targeting sialyl Lewis A mediate tumor clearance through distinct effector pathways. *J. Clin. Invest.* **129**, 3952–3962 (2019).
34. D. D. Engle *et al*., The glycan CA19-9 promotes pancreatitis and pancreatic cancer in mice. *Science* **364**, 1156–1162 (2019).
35. S. Chen *et al*., Combination of 4-1BB agonist and PD-1 antagonist promotes antitumor effector/memory CD8 T cells in a poorly immunogenic tumor model. *Cancer Immunol. Res.* **3**, 149–160 (2015).
36. S. Kleffel *et al*., Melanoma cell-intrinsic PD-1 receptor functions promote tumor growth. *Cell* **162**, 1242–1256 (2015).
37. K. Monroe *et al*., "Anti-siglec-7 antibodies and methods of use thereof." Patent WO/2017/040301Al (2017), US20200277374A1 (pending).
38. S. Cornen, B. Rossi, N. Wagtmann, "Siglec neutralizing antibodies." Patent WO/2017/153433Al (2017), US20190085077A1 (pending).
39. F. Nimmerjahn, J. V. Ravetch, Divergent immunoglobulin g subclass activity through selective Fc receptor binding. *Science* **310**, 1510–1512 (2005).
40. Z. Granot *et al*., Tumor entrained neutrophils inhibit seeding in the premetastatic lung. *Cancer Cell* **20**, 300–314 (2011).
41. E. S. Dellon *et al*., Anti-Siglec-8 antibody for eosinophilic gastritis and duodenitis. *N. Engl. J. Med.* **383**, 1624–1634 (2020).
42. M. P. Lenza, U. Atxabal, I. Oyenarte, J. Jiménez-Barbero, J. Ereño-Orbea, Current status on therapeutic molecules targeting Siglec receptors. *Cells* **9**, 2691 (2020).
43. C. S. Delaveris, S. H. Chiu, N. M. Riley, C. R. Bertozzi, Modulation of immune cell reactivity with *cis*-binding Siglec agonists. *Proc. Natl. Acad. Sci. U.S.A.* **118**, e2012408118 (2021).
44. F. Li, J. V. Ravetch, Inhibitory Fcγ receptor engagement drives adjuvant and anti-tumor activities of agonistic CD40 antibodies. *Science* **333**, 1030–1034 (2011).
45. R. Dahan *et al*., FcγRs modulate the anti-tumor activity of antibodies targeting the PD-1/PD-L1 Axis. *Cancer Cell* **28**, 543 (2015).
46. F. Nimmerjahn, P. Bruhns, K. Horiuchi, J. V. Ravetch, R. Fcgamma, FcgammaRIV: A novel FcR with distinct IgG subclass specificity. *Immunity* **23**, 41–51 (2005).